© creative

Scientific paper

Inhibition Effect of Benzimidazole Derivatives on the Corrosion of Mild Steel in Acidic Medium: Experimental and Theoretical Studies

Sonia Benabid^{1,*} and Linda Toukal²

¹ Laboratory of Electrochemistry of Molecular and Complex Materials (LEMMC), Department of Process Engineering, Faculty of Technology, Ferhat Abbas University Setif-1, Setif 19000, Algeria

² Laboratory of Electrochemistry and Materials (LEM), Department of Engineering Process, Faculty of Technology, Ferhat Abbas University Setif-1, Setif 19000, Algeria

* Corresponding author: E-mail: sonia_benabid@yahoo.fr Tel: +213552755767

Received: 08-08-2024

Abstract

The effect of heterocyclic compounds, derived from benzimidazole (BnZ), namely1-Benzyl-2-phenyl 1H-benzimidazole (BI) and 1-(4-Nitrobenzyl)-2-(4-nitrophenyl)-1H-benzimidazole (NNBI), on the carbon corrosion steel in 1M HCl medium was assessed by electrochemical impedance spectroscopy (EIS) and potentiodynamic polarization (PDP). The effects of the concentration and the temperature were studied. The determined electrochemical parameters showed that the two inhibitors are of mixed type. The inhibition efficiency of NNBI was lesser than that of BI. The most electron-withdrawing substituent offers the lowest efficiency. The mechanism of action of these inhibitors has been defined by the thermodynamic study. Calculated ΔG°_{ads} , E_{a} , ΔH°_{a} , and ΔS°_{a} values confirmed that BI and NNBI adsorb through a chemical and physical process. The adsorption process was found to be spontaneous and followed the Langmuir adsorption isotherm. The quantum chemical parameters calculated by density functional theory (DFT) and molecular dynamics simulation (MDS) corroborate both the experimental data and those of the literature.

Keywords: Corrosion; steel; organic inhibitors; benzimidazole; DFT; MDS.

1. Introduction

Acid solutions widely used in various industrial processes (e.g., acid pickling, acid cleaning, oil well acidification, and acid descaling) cause severe corrosion of mild steel.

A number of physical, chemical, and mechanical properties favor the use of mild steel (MS) for construction and manufacturing purposes. Since MS is mainly used as structural and instrumental material, which often needs to use acids such as hydrochloric acid for pickling, descaling and various petrochemical processes, the prevention of its corrosion is necessary. The use of organic corrosion inhibitors has proven to be the most practical and effectives methods for protecting metals against corrosion in acidic media.

During the last few decades, benzimidazole (BnZ) and its non-toxic derivatives have attracted considerable

attention due to their inhibitive action which proceeds via their adsorption on the metal surface by displacing pre-adsorbed water molecules at the interface forming subsequently an isolating barrier film. The adsorption of these heterocyclic compounds on the metal surface occurs due to the interaction of their unshared electron pairs on nitrogen atoms and the π -electrons in the phenyl rings with d-orbitals of the metal surface. These electronic features contribute to their effectiveness as corrosion inhibitors.

This paper deals with the study of the inhibition efficiency of two benzimidazole derivativesnamely1-Benzyl-2-phenyl-1H-benzimidazole (BI) and 1-(4-Nitrobenzyl)-2-(4-nitrophenyl)-1H-benzimidazole (NNBI) against the corrosion of mild steel in 1 M HCl medium.

The molecular structures of the inhibitors BI and NNBI are shown in Fig. 1.

Figure 1. Molecular structures of 1-Benzyl-2-phenyl-1H-benzimidazole (BI) and 1-(4-Nitrobenzyl)-2-(4-nitrophenyl)-1H-benzimidazole (NNBI) inhibitors

To ensure a deep understanding of the process of corrosion prevention, various experimental techniques such as potentiodynamic polarization (PDP) and electrochemical impedance spectroscopy (EIS) were performed. The thermodynamic and kinetic parameters were determined and discussed. The electronic properties of tested compounds and their interactions with the iron surface were obtained from theoretical studies using DFT and MD simulations. The theoretical and experimental results corroborate.

2. Experimental

2. 1. Materials and Solutions

The mild steel XC52 used in this study was determined from its technical sheet supplied by Sonatrach which is a big oil company located in Hassi Messaoud (southern Algeria).

The chemical composition (wt. %) of the mild steel was: C = 0.1038, Si = 0.1261, Mn = 0.971, P = 0.002, S = 0.0021, Cr = 0.01, Mo = 0.005, Ni = 0.005, Al = 0.0032, Co = 0.50, Cu = 0.01, No = 0.0419, Ti = 0.0025, V = 0.005, W = 0.05, Sn = 0.005, Sn

A conventional three-electrode cell was used for the electrochemical experiments. A platinum plate with a surface area of 1cm² served as the counter electrode and Ag/AgCl as reference electrode. The working electrode is a square shaped mild steel coated with Teflon so that only the cross section (0.25 cm²) is exposed to the acid solution.

For reliable and reproducible data, the surface of the working electrode was mechanically polished prior to each test (before immersion in the acid solution), using abrasive Silicon Carbide (SiC) paper of increasingly fine particle size (i.e., 180, 320, 600, 800, 1000, 1200 and 2500), followed by rinsing with double distilled water (ddH $_2$ O), degreasing with acetone and finally drying at room temperature.

The test solution 1 M HCl, was prepared from analytical grade reagent HCl (37%) purchased from Sigma

Aldrich and distilled water. Four different concentrations $(5 \times 10^{-6}, 1 \times 10^{-5}, 5 \times 10^{-5} \text{ and } 1 \times 10^{-4} \text{ M})$ of the studied inhibitors were prepared for analysis. This range was determined after studying the solubility of the inhibitors in the corrosive environment.

2. 2. Electrochemical Measurements

The electrochemical measurements were performed using a set-up comprising a Voltalab40, controlled by "Voltamaster 4" analysis software, and were recorded in a three-electrode Pyrex cell. The potential applied to the sample varied continuously, with a scanning speed of 2mV/s. The working electrode potential reached stability after 30 minutes waiting period. All potentials were measured relative to the KCl-saturated Ag/AgCl reference electrode.

The electrochemical impedance diagrams were recorded in the frequency range $100~\rm kHz$ – $10~\rm Hz$ with disturbance amplitude of $10~\rm mV$.

2. 3. Quantum Chemical Study

All theoretical calculations were done with the GAUSSIAN 09 software, and the geometry of the BnZ derivatives was entirely optimized using the DFT method at the B3LYP level with base 6-31G (d, p).^{5,6}

2. 4. Molecular Dynamic Simulation Study (MDS)

MDS was realized using BIOVIA Materials Studio 8.0 software, developed by Accelrys Inc. USA.^{7, 8} In this study, we used three modules: (i) the molecular structure of the inhibitor in gas, (ii) the aqueous phase, geometrically optimized using the Forcite module, (iii) the adsorption localization module was used to identify possible adsorption configurations. A simulation box with dimensions $17.38~\text{Å} \times 17.38~\text{Å} \times 27.16~\text{Å}$, was used to determine the interaction between the studied inhibitors molecules and the

Fe (110) surface. Periodic boundary conditions were used in all three directions, and the equations of motion were integrated into the canonical (constant-volume) NVT ensemble. The Fe plate, the water plate containing the studied inhibitors, and a vacuum layer were included in the simulation box. We worked at a temperature of 298 K (about 25 °C) using the Condensed-phase Optimized Molecular Potentials for Atomistic Simulation Studies (COMPASS) force field.

3. Results and Discussion

3. 1. Electrochemical Measurements

3. 1. 1. Concentration effect of BI and NNBI by PDP

Potentiodynamic polarization experiment was performed to assess the kinetics of cathodic and anodic reactions. The polarization curves in the absence and presence of different concentrations of BI and NNBI in 1 M HCl solution at 20 °C are shown in Fig. 2.

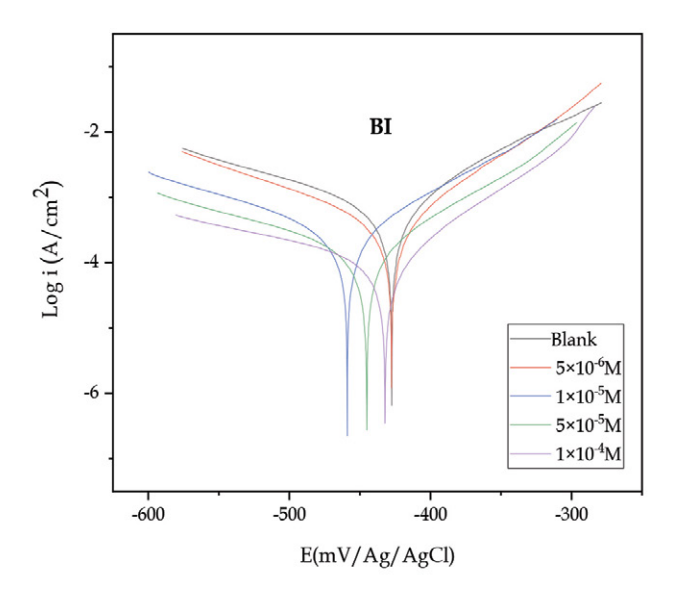


Table 1. Electrochemical parameters and corrosion inhibition efficiency of mild steel in 1M HCl in the absence and presence of different concentrations of BI and NNBI at $20~^{\circ}\text{C}$

Inhibitor	C (M)	E _{corr} (mV/Ag/ AgCl)	i _{corr} (mA/ cm ²)	β _a (mV/ dec)	β _c (mV/ dec)	IE %	θ
BI	Blank	-427	0.63	82	-159	_	_
	5×10^{-6}	-428	0.33	67	-125	48	0.48
	1×10^{-5}	-459	0.30	91	-160	52	0.52
	5×10^{-5}	-445	0.16	85	-177	75	0.75
	1×10^{-4}	-432	0.10	72	-202	84	0.84
NNBI	5×10^{-6}	-477	0.4	131	-128	37	0.37
	1×10^{-5}	-485	0.33	134	-125	48	0.48
	5×10^{-5}	-468	0.28	87	-116	56	0.56
	1×10^{-4}	-460	0.18	82	-149	71	0.71

 i^0_{corr} and i_{corr} represent the current densities in the absence and presence of BI and NNBI inhibitors, respectively.

Analysis of the potentiodynamic polarization curves (Fig. 2) reveals that increasing the concentration of both

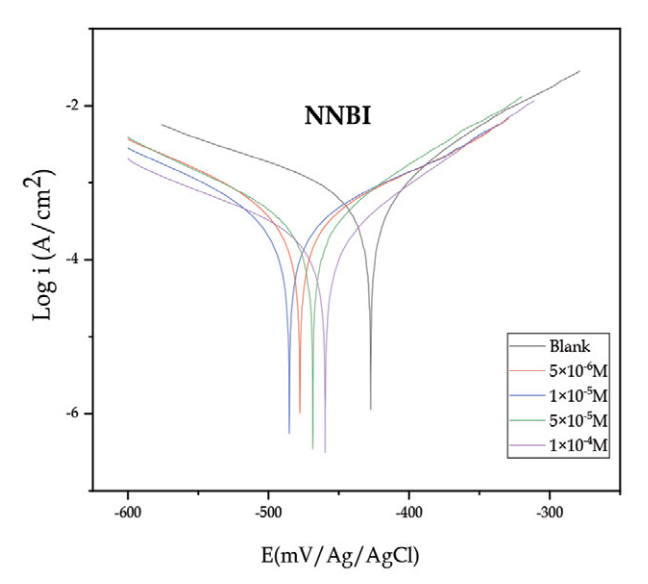


Figure 2. Polarization curves of mild steel in 1 M HCl in the absence and presence of different concentrations of BI and NNBI at 20 °C.

The electrochemical parameters such as the corrosion potential (E_{corr}), the current densities (I_{corr}), the cathodic and anodic tafel slopes (β_c and β_a), the surface coverage rate (θ) and the inhibitory efficiency (IE %) are listed in Table 1.

The inhibition efficacy (IE %) and the surface coverage rate (θ) of BI and NNBI were determined from the two equations below:

IE % =
$$\left(\frac{i_{corr}^0 - i_{corr}}{i_{corr}^0}\right) \times 100$$
 (1)

$$\theta = \begin{pmatrix} \frac{i_{corr}^0 - i_{corr}}{i_{corr}^0} \end{pmatrix} \tag{2}$$

inhibitors causes a decrease in cathodic and anodic current densities. This result suggests that the addition of BI and NNBI reduces anodic dissolution and also retards the hydrogen evolution. This phenomenon is due to the creation of an inhibitor barrier between the corrosive medium and the metal surface.⁹

Inspection of Table 1 shows that the corrosion potential (E_{corr}) of BI and NNBI shifts towards negative values in comparison with the corrosion potential of the blank solution. This shift is less than 85 mV, suggesting that BI and NNBI act as mixed type inhibitor with predominance on the cathodic reaction.¹⁰

On the other hand, the values of both anodic and cathodic Tafel slopes (β_a , β_c) slightly change when the concentration of the inhibitors increases, which means that the

addition of inhibitors reduces the anodic dissolution of mild steel as well as retards the cathodic hydrogen evolution reaction without affecting the reactions mechanism. 10,11

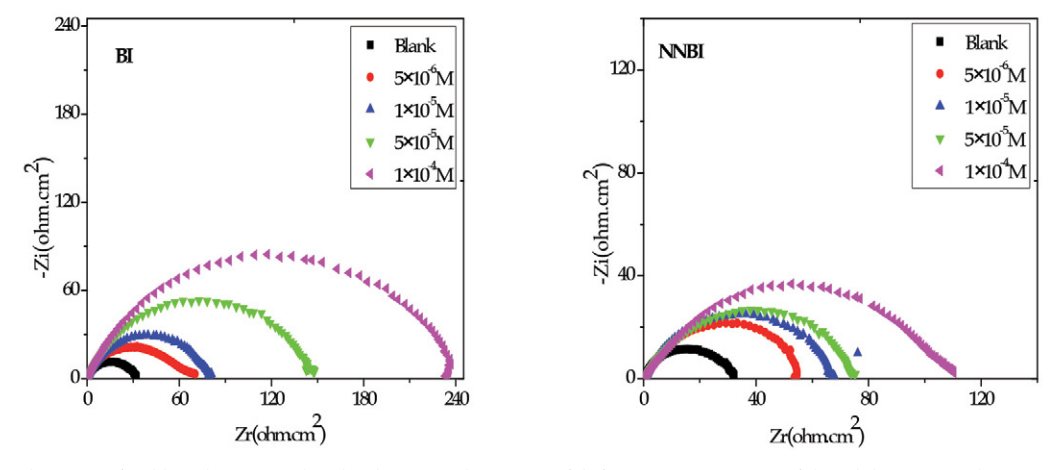


Figure 3. Nyquist diagrams of mild steel in 1M HCl in the absence and presence of different concentrations of the inhibitors BI and NNBI at 20 °C.

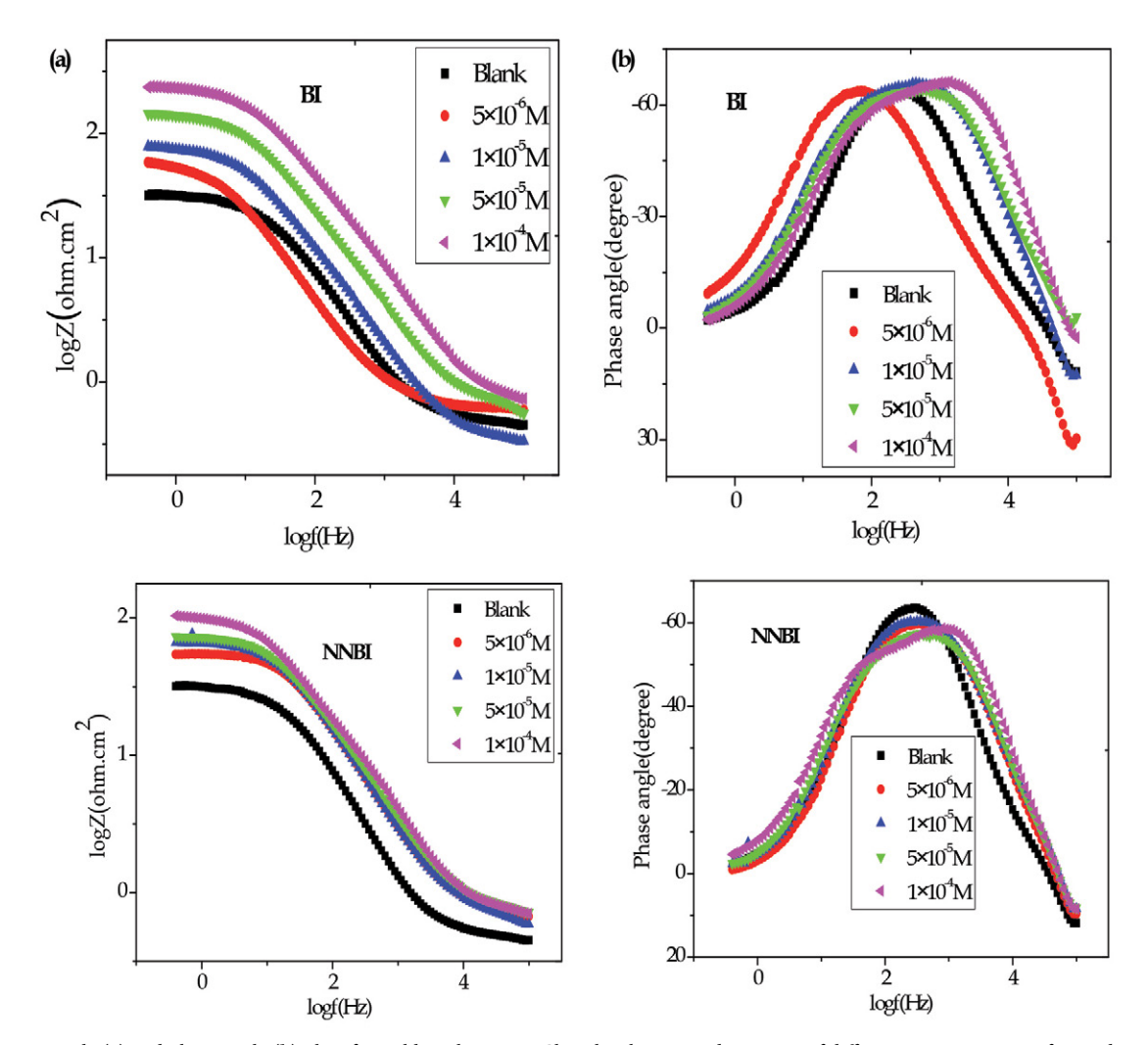


Figure 4. Bode (a) and phase angle (b) plots for mild steel in 1M HCl in the absence and presence of different concentrations of BI and NNBI at 20 °C.

3. 1. 2. Concentration Effect of BI and NNBI by EIS

In order to evaluate the electrochemical phenomenon which occurs at the metal/solution interface, Nyquist plots of mild steel in 1 M HCl in the absence and presence of various concentrations of BI and NNBI at 20 °C are represented in Fig. 3.

We can notice that for all concentrations, the presence of a single capacitive loop corresponding to the charge transfer resistance (R_{ct}) generally indicates that the dissolution reaction of XC52 in 1 M HCl is controlled by a single process charge transfer which is not affected by the presence of inhibitors. ¹² Nyquist curves are not perfect semicircles due to the heterogeneity of the electrode surface. This heterogeneity can result from the surface roughness, impurities, dislocations, grain boundaries, adsorption and desorption phenomena of the inhibitor. ^{13,14}

The Bode diagrams (Fig. 4) reveals the existence of an equivalent circuit containing a single constant phase element in the metal/solution interface. The increase in absolute impedance at low frequencies in the Bode plots confirms that the protection is better at high inhibitor concentrations. The observation of a single-phase peak in the central frequency range indicates the existence of a unique constant, linked to the electrical double layer.¹⁵

To define a model for the steel/solution interface in the absence and presence of the inhibitors BI and NNBI, the data obtained by EIS were adjusted to the electrical equivalent circuit, as illustrated in Fig. 5.

$$R_s$$

Figure 5. Equivalent electrochemical circuit representing the steel/solution interface used for the simulation of BI and NNBI impedance diagrams.

Where R_c is the solution resistance, R_{ct} denotes the charge transfer resistance, and CPE is the constant phase element which replaces the double layer capacitance (C_{dl}) allowing a more precise fit to the experimental results.

The double layer capacitance (C_{dl}) is obtained through the following equation (3):

$$C_{dl} = \frac{1}{2\pi f_{max}} \times \frac{1}{R_{ct}} \tag{3}$$

Where f_{max} is the frequency with maximal impedance of the imaginary component.

The inhibition efficiency is calculated from the following formula (4):

IE (%) =
$$\frac{R_{ct} - R_{ct}^0}{R_{ct}} \times 100$$
 (4)

Where R^0_{ct} and R_{ct} represent the charge transfer resistances in the absence and presence of the inhibitors BI and NNBI, respectively.

From the diagrams of Nyquist, the values of (R_s) , (R_{ct}) , (C_{dl}) , and consequently the inhibition efficiency (IE) of BI and NNBI were obtained. These different impedance parameters are summarized in Table 2.

Table 2. Electrochemical impedance parameters for mild steel in 1 M HCl in the absence and presence of different concentrations of BI and NNBI at 20 °C.

Inhibitor	C (M)	R_s $(\Omega \text{ cm}^2)$	R_{ct} $(\Omega \text{ cm}^2)$	C_{dl} $(\mu F/\text{cm}^2)$	<i>IE</i> (%)
BI	Blank	0.368	32	249	_
	5×10^{-6}	0.24	67	597	52
	1×10^{-5}	0.29	80	199	60
	5×10^{-5}	0.7	146	98	78
	1×10^{-4}	1	237	48	87
NNBI	5×10^{-6}	1	54	147	41
	1×10^{-5}	0.83	67	136	52
	5×10^{-5}	1	74	132	57
	1×10^{-4}	1.7	108	117	70

Examination of Table 2 shows that the addition of 1×10^{-4} M of BI and NNBI inhibitors augmented the values of R_{ct} . This increase can be attributed to the adsorption of the inhibitors on the metal surface by forming a protective layer against immediate exposure to the aggressive acidic microenvironment. On the other hand, (C_{dl}) , in the presence of the inhibitors decreased compared to that of the solution without inhibitors; this decrease may be due to the displacement of the water molecules present at the metallic interface in favor of the adsorbed BI and NNBI molecules. Indeed, there is a positive correlation between the adsorption of the inhibitors and the thickness of the organic deposit, whereas the capacity of the double layer decreases proportionally. 14

3. 1. 3. Temperature Effect

Temperature is one of the crucial steel behavior-modifying factors in a corrosive environment; Thereby, it can alter the nature of the metal/inhibitor interaction. Increasing temperature can impact significantly the formation of the inhibitor film. Indeed, a rise in temperature would promote the inhibitor desorption as well as a quick dissolution of the formed organic compounds or complexes, subsequently causing a weakening of the steel corrosion resistance.¹⁷

In order to analyze the effect of temperature on the inhibition efficiency of BI and NNBI, polarization curves of mild steel in 1 M HCl solution, without and with ad-

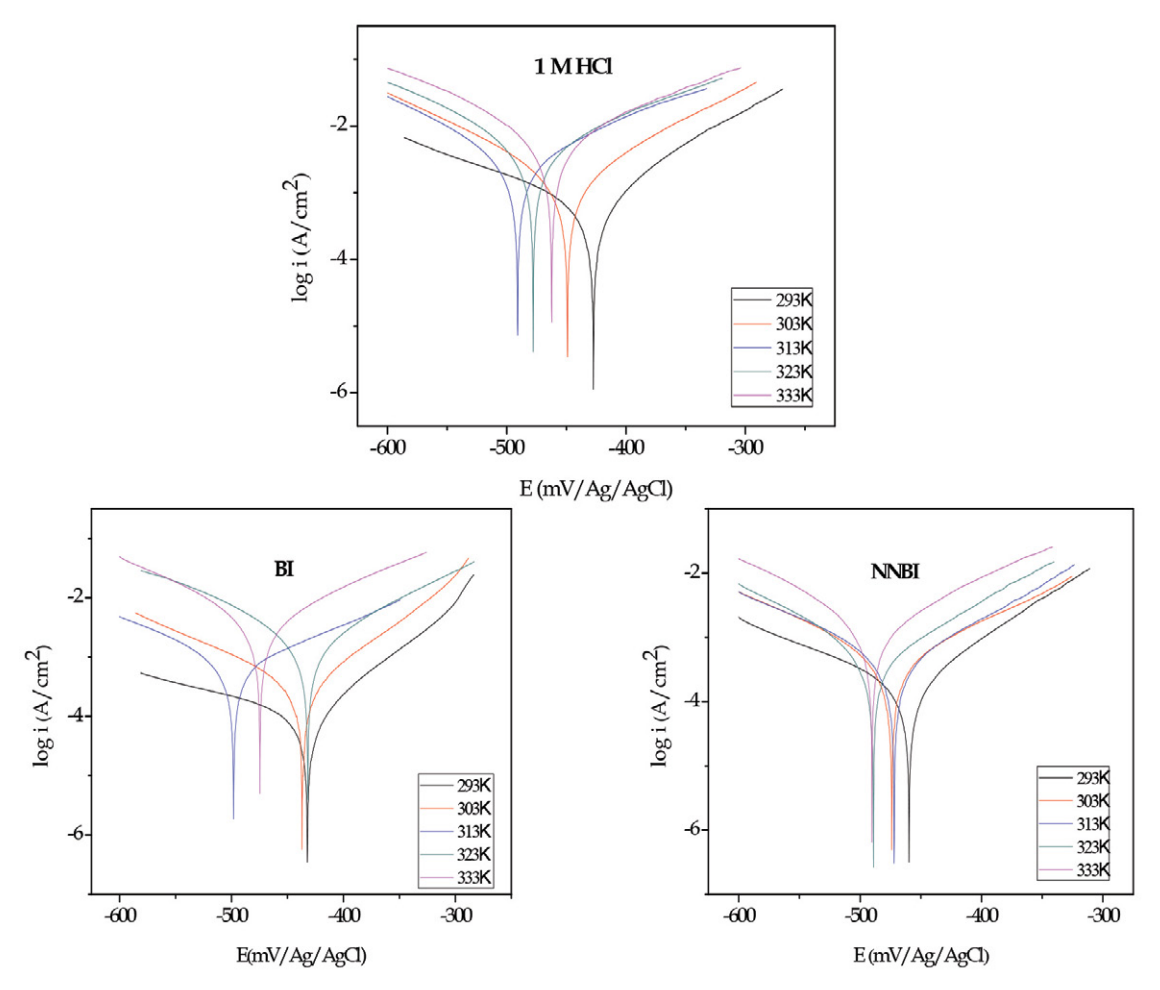


Figure 6. Tafel curves for corrosion of mild steel in 1 M HCl in the absence and presence of 1×10^{-4} M of BI and NNBI at different temperatures.

Table 3. Influence of temperature on the electrochemical parameters of mild steel in 1 M HCl medium in the absence and presence of $1\times10^{-4}\,\mathrm{M}$ of BI and NNBI

Te	emperature (K)	E _{corr} (mV/Ag/ AgCl)	i _{corr} (mA/ cm ²)	$eta_a \ (mV/dec)$	β_c (mV/dec)	IE (%)
	293	-427	0.63	82	-159	_
7	303	-449	1.76	114	-121	_
Ħ	313	-491	3.21	145	-118	_
1 M HCl	323	-478	6.13	173	-140	_
1	333	-462	8.65	168	-147	_
BI	293	-432	0.1	72	-202	84
+ >	303	-437	0.30	7	-119	83
M HCI	313	-498	0.64	134	-111	80
H.		-432	1.6	120	-137	74
1 N	333	-475	2.81	135	-126	68
	293	-460	0.18	82	-149	71
+ _	≥ 303	-474	0.52	124	-124	70
MHC	313	-472	1.1	108	-129	66
Ξ	¥ 303 50 313 323	-490	2.21	108	-109	64
=	333	-490	3.5	88	-76	60

dition of 1×10^{-4} M of BI and NNBI, were conducted at temperature ranging from 293 to 333 K as shown in Fig. 6.

The electrochemical parameters obtained from the polarization curves of mild steel in 1M HCl before and after addition of the optimal concentration $(1 \times 10^{-4} \,\mathrm{M})$ of BI and NNBI at different temperatures are shown in Table 3.

According to Table 3, we can notice that E_{corr} is altered by increasing temperatures and moves towards more negative values iccrease with increasing temperatures but they remain much lower compared to those observed for HCl alone, thereby confirming that BI and NNBI inhibit corrosion in the temperature range (293–333 K) albeit they appeared less efficient at the highest temperatures. The decrease in IE (%) with increasing temperatures is explained by the desorption of the previously adsorbed inhibitors, which leads a larger metallic surface to be exposed to the corrosive solution.¹⁸ This phenomenon may be the result of Van Der Waals interactions (weak forces) between the metal surface and the inhibitor. 19 These interactions are very sensitive to thermal agitation and are very easy to break according to increased temperatures. The increase in temperature shifts the adsorption-desorption balance toward the desorption process, thus reducing the inhibition efficiency of the compounds studied. 19,20

3. 1. 4. The Activation Parameters

Temperature is a critical factor that has a considerable effect on the behavior of steel in acidic medium. As the temperature increases, it can modify the metal/inhibitor interaction interface. To assess the impact of this parameter on the kinetics of protective film formation, the activation parameters of the corrosion process such as the activation energy (E_a), the activation enthalpy (ΔH°_a) and activation entropy (ΔS°_a) were calculated at different temperatures (293–333 K), in the absence and presence of 1 × 10^{-4} M of BI and NNBI inhibitors.

Activation energy (E_a) was determined using the i_{corr} values obtained from the polarization curves following the

equation (5):21

$$i_{corr} = Aexp\left(\frac{-E_a}{RT}\right) \tag{5}$$

Where i_{corr} is the corrosion current density, A is a pre-exponential factor, E_a denotes the activation energy, R represents the universal gas constant, and T is the temperature.

Fig. 7 represents the variation of the corrosion current density as a function 1/T (Ln $i_{corr} = f(1/T)$). This variation is a straight line both in the absence and presence of 1×10^{-4} M of BI and NNBI at different temperatures.

An alternative Arrhenius equation can determine the activation enthalpy (ΔH°_{a}) and the activation entropy (ΔS°_{a}) using the following equation (6):

$$i_{corr} = \frac{RT}{Nh} \exp\left(\frac{\Delta S_{a}^{\circ}}{R}\right) \exp\left(-\frac{\Delta H_{a}^{\circ}}{RT}\right)$$
 (6)

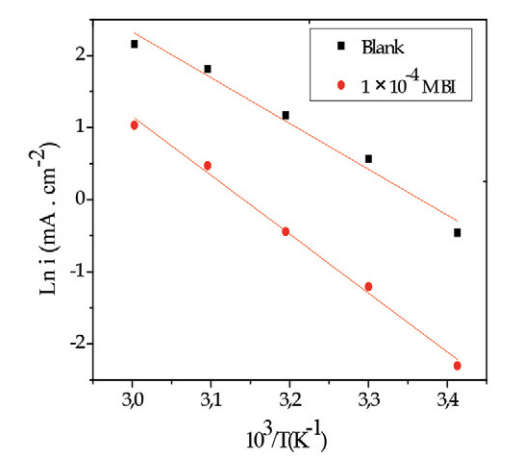
Where h is the Planck's constant, N denotes the Avogadro number, R represents the universal gas constant.

The variation of ln (i_{corr}/T) as a function 1/T is a straight line (Fig. 8), with a slope of ($-\Delta H^{\circ}_{a}/R$) and an intercept equal to ((ln R/Nh) + $\Delta S^{\circ}_{a}/R$). Therefore, it was possible to calculate ΔH°_{a} and ΔS°_{a} .

The activation parameters such as the activation energy (E_a)the activation enthalpy (ΔH°_a) and activation entropy (ΔS°_a) in the absence and presence of 1 × 10⁻⁴ M of BI and NNBI given in Table 4 are calculated from the Arrhenius relation.

Table 4. Activation parameters of the corrosion process of mild steel in 1M HCl solution in the absence and presence of 1×10^{-4} M of BI and NNBI

Inhibitor	E _a (kJ/mol)	ΔH° _a (kJ/mol)	ΔS° _a (J/mol K)
1M HCl	53.6	51.19	-72.23
$1M HCl + 1 \times 10^{-4} M BI$	69.27	66.72	-36
$1M \text{ HCl} + 1 \times 10^{-4} \text{ M NNBI}$	71.6	69	-27



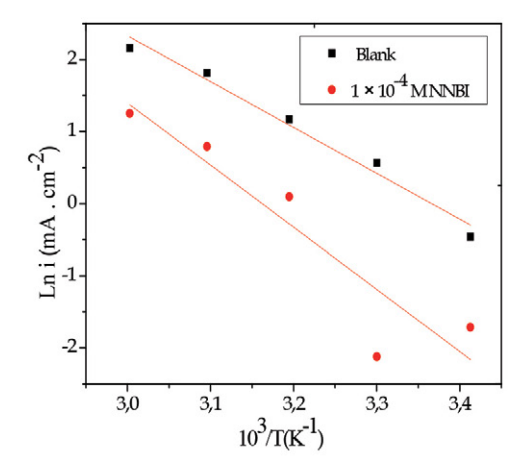
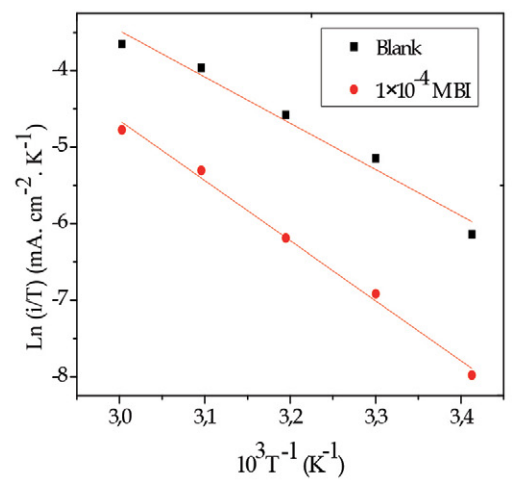


Figure 7. Arrhenius plots of the corrosion of mild steel in 1M HCl in the absence and presence of 1×10⁻⁴ M of BI and NNBI at different temperatures



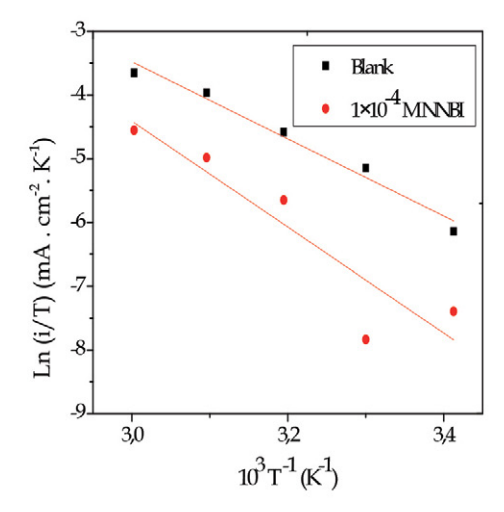


Figure 8. Alternative Arrhenius plots for mild steel in 1 M HCl in the absence and presence of 1×10^{-4} M of BI and NNBI.

From Table 4, we can observe that is higher in the presence of inhibitor compared to the blank. The increase in values in the presence of the benzimidazole derivatives is typical of the physisorption of these molecules on the steel surface.²² The high values of E_a can also be attributed to the increase in the thickness of the double layer.^{23,24} Furthermore, the augmentation of E_a after addition of BI or NNBI indicates that physisorption, through electrostatic interactions, occurred in the first step of the inhibition mechanism.²⁵ Besides, the positive signs of the enthalpies reflect the endothermic nature of the steel dissolution process. 26,27 ΔH°_{a} values closer to 100 kJ/mol imply chemisorption while those below 40 kJ/mol correspond to physisorption. In this study, the values in the presence of inhibitors are positive, similarly closer to 100 kJ/mol, and higher than those found in the solution exempt of inhibitor. This reflects a mixed type adsorption process²⁸ and shows that the dissolution of the steel is endothermic. Concordantly, higher negative values of the entropy ΔS_a° in the presence of inhibitors signifies that there was a reduction in disorder during the transformation of the reactants into the activated iron-molecule complex in the medium.^{29, 30}

3. 1. 5. Adsorption Parameters

The effectiveness of organic corrosion inhibitors principally depends on their adsorption capacity at the metal/solution interface. Therefore, it is essential to know the adsorption isotherm, a thermodynamic parameter, which can inform us about the interaction between the inhibitor and the metal surface. To identify the type of adsorption corresponding to this inhibitor, various isotherms were tested: Langmuir, Temkin and Frumkin (Fig. 9).

Based on these isotherms, the recovery rate θ is linked to the inhibitor concentration $C_{inh}^{31,32}$ following these respective equations:

$$\frac{C_{\text{inh}}}{\theta} = \frac{1}{K_{ads}} + C_{\text{inh}}$$
 Langmuir adsorption isotherm (7)

$$\exp(-2a\theta) = K_{ads} C_{inh}$$
 Temkin adsorption isotherm (8)

$$\left(\frac{\theta}{1-\theta}\right) \exp(2a\theta) = K_{\text{ads}} C_{\text{inh}}$$
 Frumkin adsorption isotherm (9)

Where a represents the interaction constant between adsorbed particles, K_{ads} denotes the adsorption equilibrium constant, and C_{inh} stands for the inhibitor concentration.

We can notice from the Fig. 9, that the Langmuir adsorption isotherm is the most appropriate for adjusting the obtained experimental results (R² close to unity), which means that the adsorption of $1\times 10^{-4}\,\mathrm{M}$ of BI and NNBI on the mild steel surface, in 1 M HCl solution at 293 K, obeys the Langmuir adsorption isotherm. In the same experimental conditions, K_{ads} and the free energy of adsorption (ΔG_{ads}°) of BI and NNBI (Table 5) were calculated from the following relations:

$$K_{ads} = \frac{1}{C_{inh}} \times \frac{\theta}{1 - \theta} \tag{10}$$

$$\Delta G_{\text{ads}}^{\circ} = -RT \ln \left(55, 5 \cdot K_{\text{ads}} \right) \tag{11}$$

Where θ denotes the surface coverage rate, C_{inh} is the inhibitor concentration, R represents the gas constant, T is the absolute temperature, and 55.5 is the concentration of water in solution (mol/L).

Table 5. Thermodynamic parameters of adsorption of $1\times10^{-4}\,M$ of BI and NNBI on mild steel in 1 M HCl solution at 293 K

Inhibitor	$K_{ads} \left(\mathbf{M}^{-1} \right)$	ΔG°_{ads} (kJ/mol)
BI	5.25×10^4	-36.24
NNBI	2.44×10^4	-34.37

The high values of K_{ads} (5.25 × 10⁴ M⁻¹ for BI and 2.44 × 10⁴ M⁻¹ for NNBI) mean that a strong adsorption of the inhibitors occurred on the steel surface.^{33,34}

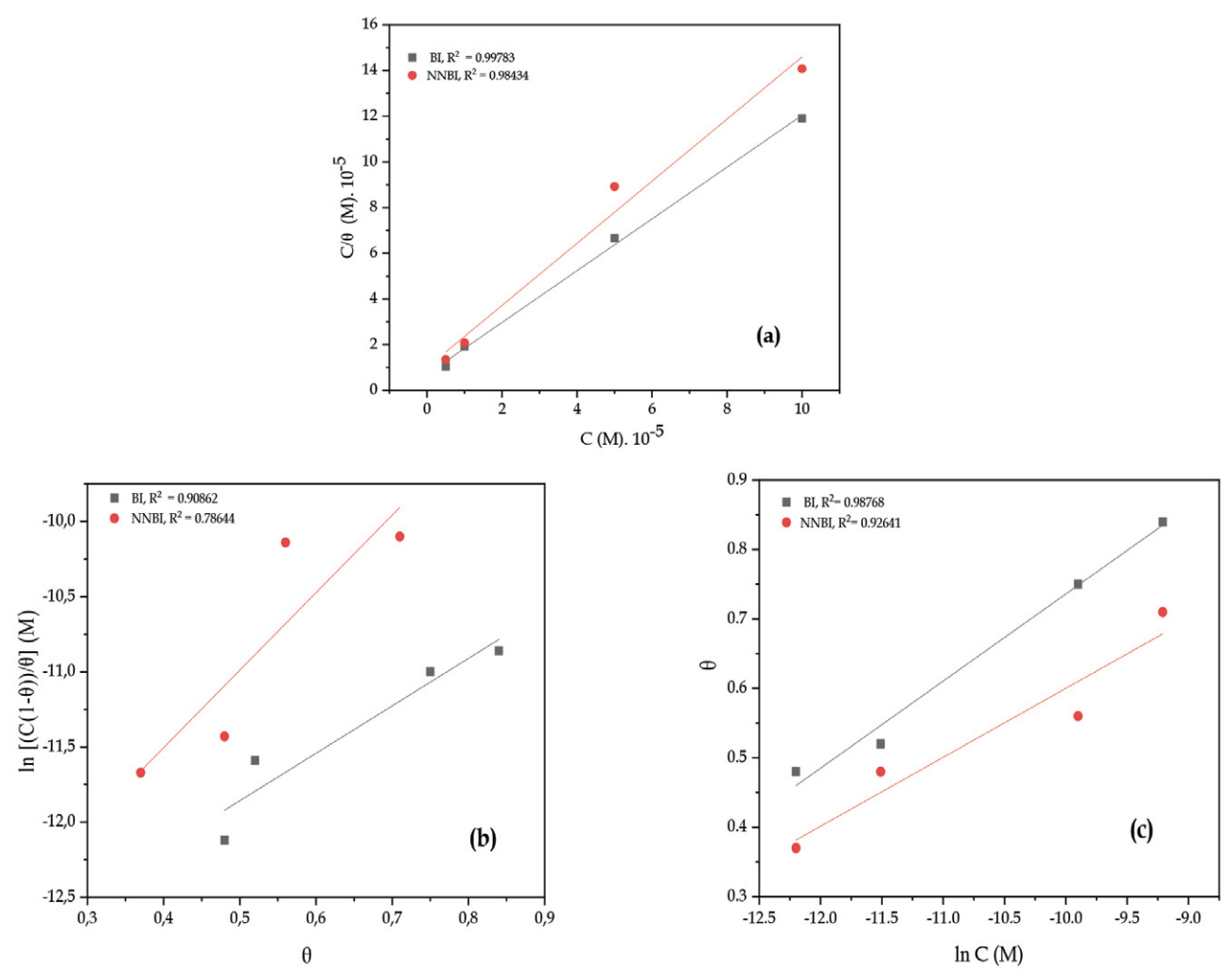


Figure 9. (a) Langmuir, (b) Fremkin and (c) Temkin adsorption isotherms for mild steel in 1 M HCl of BI and NNBI at 20 °C

The negative values of ΔG°_{ads} reflect the spontaneity of the interaction between the inhibitor, the metal surface, and the stability of the formed layer.³⁵

Furthermore, adsorption free energies ΔG°_{ads} ranged from -20 and -40 kJ/mol, which strongly suggests that the adsorption of BI or NNBI on the steel surface is a mixed type (both chemical and physical).^{36,37}

3. 2. Theoretical Study by DFT

The theoretical calculation by DFT is implemented to study the correlation between the inhibition efficiency (IE) and the molecular reactivity of the inhibitor.

The energy of the highest occupied molecular orbital (E_{HOMO}) , the energy of the lowest unoccupied molecular orbital (E_{LUMO}) , the energy gap $(\Delta E_{gap} = E_{LUMO} - E_{HOMO})$, the dipole moment (μ) , the absolute electronegativity (χ) , the absolute hardness (η) , the global softness (σ) , the number of electrons transferred (ΔN) , and the electrophilicity index (ω) were determined, 38 following equations 12–18:

$$I = -E_{HOMO} \tag{12}$$

$$A = -E_{LUMO} \tag{13}$$

Where I: Ionization potentiel (eV), A: Electron Affinity (eV).

The values of χ and η were calculated, according to Pearson:

$$\chi = (I + A)/2 \tag{14}$$

$$\eta = (I - A)/2 \tag{15}$$

σ, which describes the capacity of an atom to receive electrons, ¹³ was estimated by:

$$\sigma = 1/\eta \tag{16}$$

 ΔN is calculated as follows:

$$\Delta N = (\chi_{Fe} - \chi_{inh})/2 (\eta_{Fe} + \eta_{inh})$$
 (17)

Where χ_{Fe} χ_{inh} , η_{Fe} and η_{inh} designate the absolute electronegativity and the absolute hardness of iron and inhibitor, respectively.

The theoretical values χ and η of iron are equal to 7 and 0 eV. mol $^{-1}$ respectively. 40

Eventually, ω was obtained as follows:

$$\omega = \chi^2 / 2\eta \tag{18}$$

Adsorption on the metal surface is due to donor-acceptor interactions between the π electrons of the inhibitor and the vacant d orbitals on the surface atoms of the metal.⁴¹

The electron donor (molecule having a high E_{HOO}) interacts with a suitable acceptor (molecule having a low E_{LUMO}). Thus, high values of E_{HOMO} facilitate the adsorption of the inhibitor to the metal surface by influencing the electronic transfer process through the adsorbed layer. On the other hand, E_{LUMO} highlights on the electron acceptor character of the molecule (e.g., inhibitor).

The decrease in the E_{LUMO} value is an indicator of the ability of the molecule to accept electrons from the metal surface. ⁴² As established in the literature, a good corrosion inhibitor is often the one which not only gives up its electrons, but is also capable of accepting electrons from the metallic surface; the lower the E_{LUMO} is, the higher the IE.

The gap between the E_{HOMO} and E_{LUMO} is another important parameter; the low values of ΔE_{gap} are a sign of good inhibitory activity.⁴³ A high ΔE_{gap} value characterizes a hard molecule and a low ΔE_{gap} value characterizes a soft one

Hard molecules are facing difficulties to donate electrons to an acceptor, and consequently their reactivity is lower than that of soft molecules. Adsorption occurs in the molecular region where σ has the highest value.²⁵ IE increases with increasing values of but with decreasing values of ω .

According to Lukovits, if ΔN < 3.6, the inhibitor is an electron donor and therefore it is a valuable inhibitor, since its IE increases with its capacity to donate electrons.⁴⁴

The dipole moment is mostly used to describe the molecular polarity.⁴⁵ Organic compounds with high dipole moments are good inhibitors.⁴⁶

The optimized molecular structures and the frontier molecular orbital density distributions of the organic compounds BI and NNBI are represented in Fig. 10.

Fig. 10 shows that the HOMO density distribution on the BI molecule is identical to that of LUMO, centered essentially on the planar benzimidazole group and its phenyl substituent bonded to C13.⁴⁷ For the NNBI molecule,

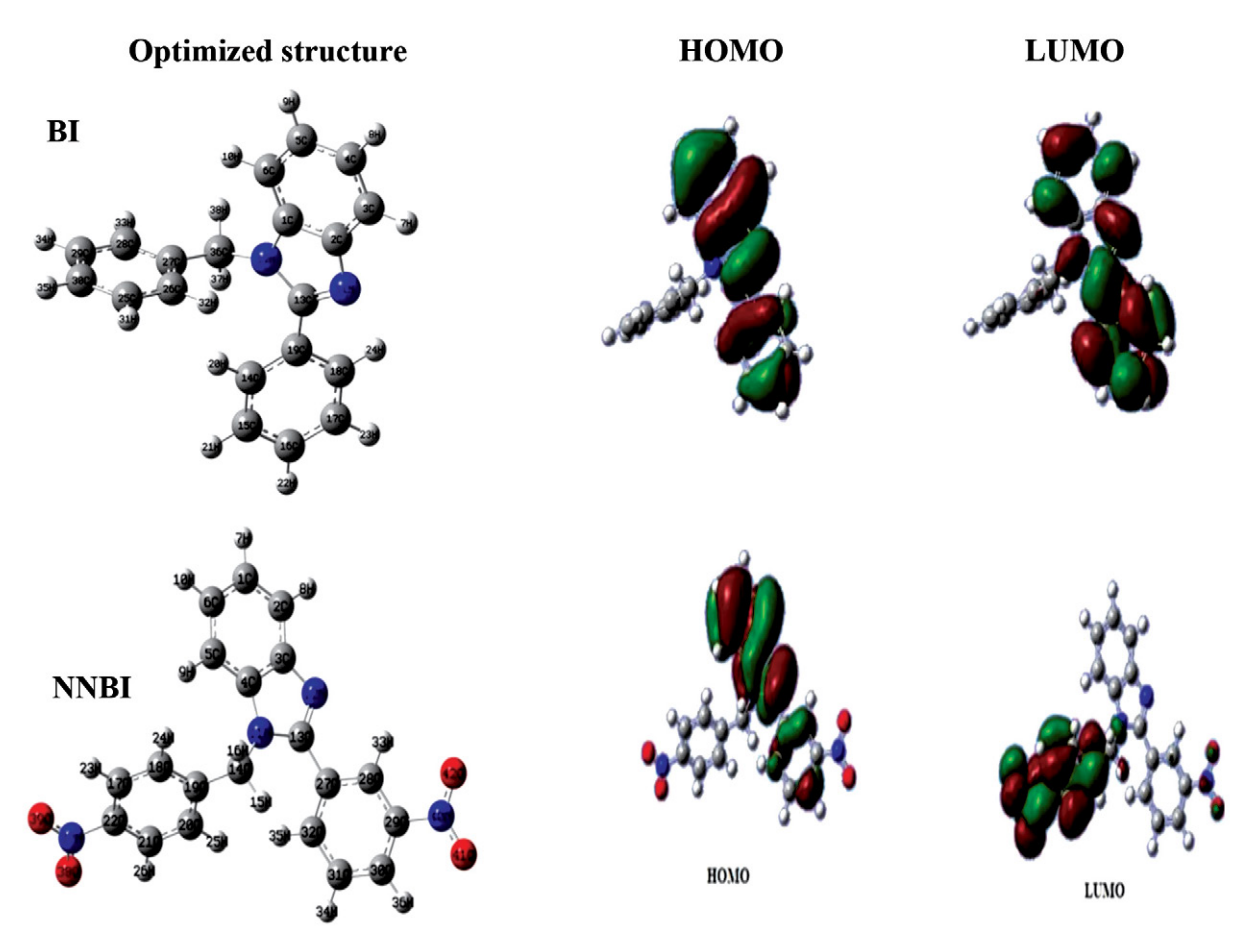


Figure 10. Optimized molecular structures and the frontier molecular orbital density distributions of the organic compounds BI and NNBI given by B3LYP/6-31G (d, p).

the HOMO density is located mostly on the planar benzimidazole ring and on some atoms of the phenyl group bonded to C13, while the LUMO density is centered on the N11 nitrogen of benzimidazole, the nitro group of phenyl linked to C13 and nitro group, and the phenyl linked to C14.⁴⁸

The quantum parameters of BI and NNBI in the gas and aqueous phases have been summarized in Table 6.

Table 6. Quantum parameters of BI and NNBI in gas and aqueous phase calculated by DFT (B3LYP) using the 6-31G basis (d, p).

Parameters	BI		NNBI	
	gas phase	aqueous phase	gas phase	aqueous phase
$E_{tot}(eV)$	-23981.67	-23981.95	-35111.14	-35111.14
$E_{\mathrm{HOMO}}\left(\mathrm{eV}\right)$	-5.72	-6	-6.34	-6.21
$E_{\text{LUMO}}\left(\text{eV}\right)$	-1	-1.07	-2.74	-2.70
ΔE_{gap} (eV)	4.72	4.94	3.60	3.50
μ (Debye)	3.45	4.97	4.21	5.69
η (eV)	2.36	2.47	1.80	1.75
$\sigma (eV^{-1})$	0.42	0.40	0.55	0.57
χ (eV)	3.36	3.55	4.54	4.46
ω (eV)	2.4	2.54	5.73	5.67
ΔN	0.77	0.70	0.68	0.72

The data in the Table 6 show that BI and NNBI have high HOMO (-05.72 and -06.34 eV for BI and NNBI, respectively) and low LUMO energies, as well as low energy gap (ΔE) implying easy adsorption to the steel surface and consequently high inhibition efficacy (IE). This property is confirmed by the high dipole moment (μ) values (3.45)

and 4.21 Debye for BI and NNBI, respectively); these inhibitors can therefore easily transfer electrons to the vacant d orbitals of iron. Molecular reactivity depend on the hardness (n) which was found low (2.36 and 1.80 eV for BI and NNBI, respectively) and softness (σ), which was found high (0.42 and 0.55 eV for BI and NNBI, respectively).⁴⁹ The electronegativity (χ) values (3.36 and 4.54 eV for BI and NNBI, respectively) were lower than that of iron, which implied a transfer of electrons from the HOMO orbital of the inhibitor to the empty 3d orbital of iron.⁵⁰ BI and NNBI displayed ΔN values lowerthan 3.6 (0.77 and 0.68 for BI and NNBI, respectively), which indicate that they are electron donors and the metal surface is an acceptor. The IE increases with the ability of the molecule to donate electrons to the steel surface, this ability follows the sequence BI > NNBI, which is in accordance with previous data.51

The global electrophilicity index (ω) reflects the ability of a chemical species to accept electrons. A high value of electrophilicity index describes a good electrophile while a small one describes a good nucleophile. The electrophilicity indices (ω) of NNBI being higher than BI (2.4 and 5.73 eV for BI and NNBI, respectively) confirms the electrophilic nature of NNBI especially since it includes an electron-withdrawing NO₂ group in its structure.⁵²

Molecular electrostatic potential (MEP) was used to identify electrophilic and nucleophilic sites (Fig. 11). In the case of BI, the electron-rich regions are located around the heteroatoms and the conjugated double bonds. The nucleophilic active sites that promote nucleophilic reactions in the corrosion inhibition process of mild steel are the nitrogen atom N11 and the electrons of the conjugated double bonds. ⁵³ In the case of NNBI, the nucleophilic ac-

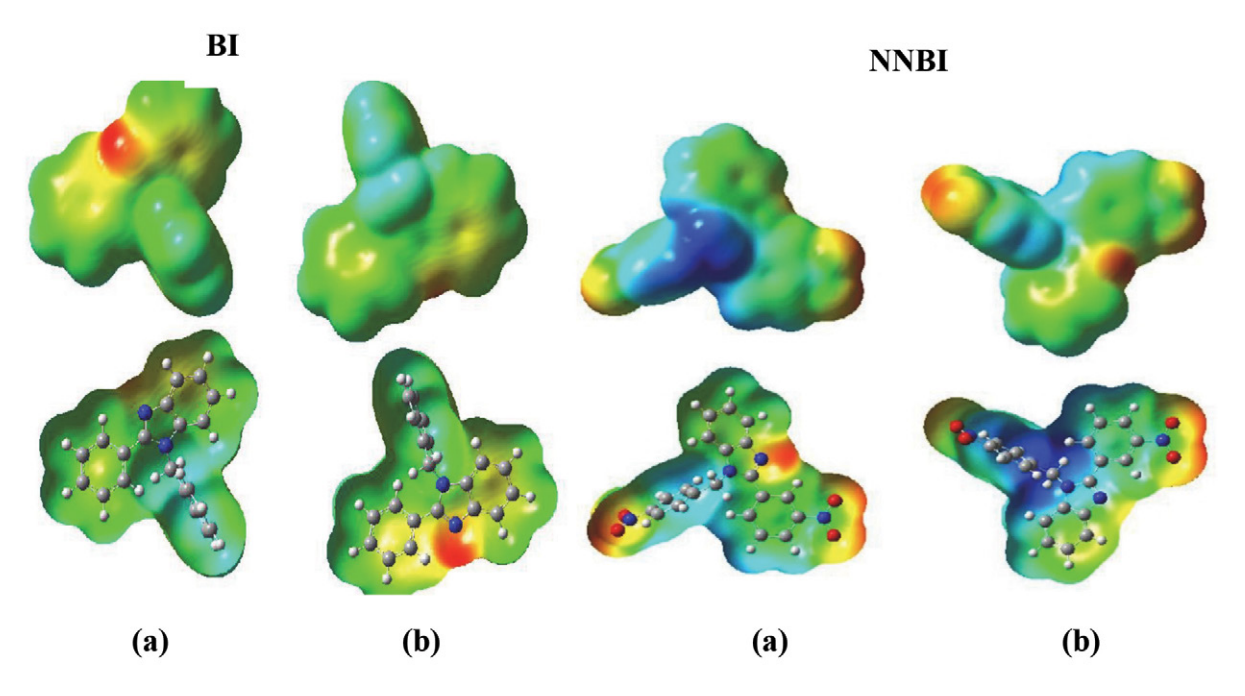


Figure 11. MEP map and counter plot of BI and NNBI inhibitors. (a) Front view and (b) Rear view.

tive sites are located on one of the nitrogen atoms and on the oxygen atoms of the two nitro groups of the substituted phenyl.⁵⁴

The distribution of Mulliken charges for BI and NNBI is shown in Table 7.

The Mulliken analysis, that estimates the adsorption centers of inhibitors, was mainly used for the calculation of the charge distribution across the entire backbone of the molecule. In the case of the BI, N11 and N12 atoms displayed negative charges with a high electron density, which means that they behave like nucleophilic centers when they interact with the mild steel surface.⁵⁵

The nitrogen and carbon atoms of the benzimidazole ring of BI exhibited negative charges, making them ideal sites for adsorption on mild steel. 53 In the case of the NNBI, we can observe that all the nitrogen and oxygen atoms have significant negative charges (–0.541, –0.389, –0.385, –0.390, –0.384 for N11, O38, O39, O41 and O42, respectively) and negative charges on some carbon atoms of the imidazole ring like C29 (–0.137) and C17 (–0.135). This indicates that these atoms are the likely active sites for the adsorption of NNBI on the mild steel surface. As a result, the NNBI molecules form a barrier, thereby preventing the arrival of aggressive ions at the metal surface, and thus reducing the rate of corrosion.

Table 7. Mulliken atomic charges calculated for BI and NNBI.

	BI			NNBI	
Atom	Gas phase	Aqueous phase	Atom	Gas phase	Aqueous phase
C1	-0.087	-0.101	C1	0.226	0.221
C2	-0.131	-0.151	C2	0.284	0.283
C3	0.249	0.246	C3	-0.121	-0.133
C4	0.197	0.196	C4	-0.095	-0.110
C5	-0.117	-0.129	C5	-0.099	-0.112
C6	-0.108	-0.119	C6	-0.118	-0.136
H7	0.088	0.106	H7	0.096	0.113
H8	0.097	0.105	H8	0.095	0.110
Н9	0.156	0.172	Н9	0.107	0.113
H10	0.086	0.109	H10	-0.546	-0.575
N11	-0.554	-0.564	N11	-0.541	-0.551
N12	-0.527	-0.557	N12	0.400	0.408
C13	0.387	0.391	C13	0.151	0.157
C14	-0.107	-0.108	C14	-0.127	-0.130
H15	0.119	0.136	H15	-0.087	-0.084
H16	0.131	0.137	H16	0.257	0.264
C17	-0.100	-0.112	C17	-0.135	-0.126
C18	-0.167	-0.182	C18	-0.066	-0.059
C19	0.120	0.108	C19	0.140	0.139
C20	-0.136	-0.147	C20	0.145	0.150
C21	-0.078	-0.094	C21	0.146	0.156
C22	-0.085	-0.102	C22	0.011	0.013
H23	0.073	0.096	H23	-0.119	-0.118
H24	0.152	0.157	H24	0.095	0.109
H25	0.076	0.096	H25	0.153	0.176
H26	0.085	0.102	H26	0.092	0.118
C27	0.093	0.091	C27	0.023	0.017
C28	-0.107	-0.120	C28	0.034	0.036
C29	-0.090	-0.101	C29	-0.137	-0.132
C30	-0.077	-0.088	C30	0.269	0.275
C31	-0.093	-0.105	C31	-0.094	-0.095
C32	-0.124	-0.131	C32	-0.109	-0.113
H33	0.119	0.114	H33	0.119	0.131
H34	0.093	0.112	H34	0.139	0.142
H35	0.091	0.112	H35	0.139	0.142
H36	0.106	0.112	H36	0.107	0.132
H37	0.081	0.117	N37	0.107	0.365
H38	0.091	0.098	O38	-0.389	-0.418
1130	0.090	0.090	O39	-0.385	-0.416
			N40	0.357	0.368
			O41	-0.390	-0.417
			O41	-0.384	-0.417
			042	-0.304	-0.413

3. 3. Molecular Dynamic Simulation Study (MDS)

For a better understanding of the interactions between BI, NNBI and the Fe (110) surface, MDS was carried out in the presence or absence of solvent molecules ($\rm H_2O$). The equilibrium adsorption configurations of BI and NNBI on the Fe (110) surface, using of the Monte Carlo simulation, are illustrated in Fig. 12.

According to Fig. 12, it clearly appears that BI and NNBI adsorb in a parallel manner to the Fe (110) surface. The nitrogen atoms in BI and NNBI molecules can donate electrons to unoccupied iron d orbitals to form coordination bonds while the electron orbitals of aromatic rings can accept electrons from the iron orbitals to form coordination bonds.⁵⁶

The descriptors obtained by the MDS for BI and NNBI on the Fe (110) surface, are listed in Table 8.

The interaction (adsorption) energy (E_{inter}), between the inhibitor and the Fe (110) surface was calculated by the following equation: ⁵⁷

Table 8. Molecular dynamics simulation (MDS) results for the lowest adsorption configurations of BI and NNBI compounds on the Fe (110) interface.

Systems		BI/Fe (110)	NNBI/Fe (110)
Total energy (E_s)	(kJ/mol)	-105	-153
Adsorption energy (E_{ads})	(kJ/mol)	-216	-405
Rigid adsorption energy	(kJ/mol)	-122	-151
Deformation energy (D_E)	(kJ/mol)	-93	-254
dE_{ads}/dN_i	(kJ/mol)	-216	-405

$$E_{inter} = E_{tot} - (E_{surf+sol} + E_{inh}) \tag{19}$$

Where, E_{tot} is the total energy of the iron crystal with the adsorbed inhibitor molecule, (E_{inter}) is the interaction energy, $E_{surf+sol}$ represents the energy of the iron surface with H_2O molecules, and E_{inh} denotes the energy of the free inhibitor molecule.

The binding energy is the negative value of E_{inter} . The total energy is defined as the sum of the rigid adsorption

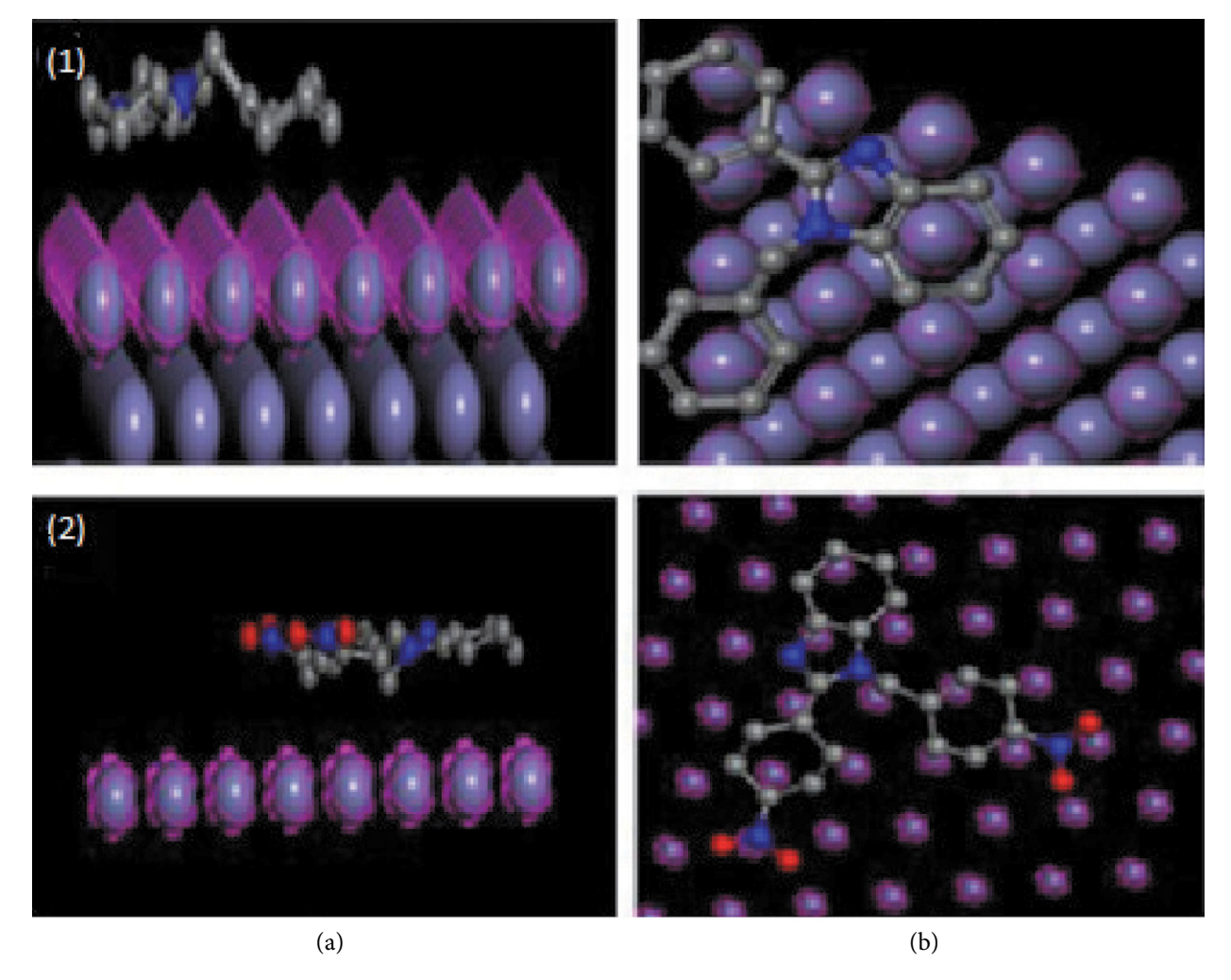


Figure 12. Equilibrium adsorption configurations of BI (1) and NNBI (2) molecules on the Fe (110) surface, (a) side view (b) top view.

energy (R.A.E) and the deformation energy (E_{def}). R.A.E reports the energy released when unrelaxed adsorbed components (i.e., before the geometry optimization step) are adsorbed onto the substrate. E_{def} is the energy released when adsorbed components are released to the substrate surface. Adsorption energy (E_{ads}) is the energy released when relaxed inhibitor molecules are adsorbed on the metal surface. The energy of the substrate (surface of the iron) is taken equal to zero.

The differential adsorption energy (dE_{ads}/dNi) is the energy of removal of an adsorbate from a particular component.²¹

The data summarized in Table 8 shows that BI and NNBI exhibit high negative adsorption energy during the simulation process, which indicates spontaneous and stronger adsorption of the inhibitors on the steel surface.⁵⁸

MDS was performed to further study the adsorption behavior of BI and NNBI on the Fe (110) surface in aqueous phase. The most stable low-energy adsorption configurations of BI and NNBI inhibitors on a Fe (110)/50 H_2O molecules system using Monte Carlo simulations are shown in Fig. 13.

From Fig. 13, it is evident that, when adsorbed on the Fe (110) surface in the presence of water, BI and NNBI adopt a flat orientation as they approach the iron surface with close contact, thereby confirming a strong adsorption of the inhibitors on the iron surface.⁵³

The values for the outputs and descriptors of the Monte Carlo simulations are listed in Table 9. It includes the total energy, the adsorption energy, the rigid adsorption energy and the strain energy of the inhibitors adsorbed on Fe (110) in the presence of 50 water molecules, as well as the differential adsorption energies of inhibitors and water.

In all cases, the adsorption energies of BI and NNBI are much higher than those of $\rm H_2O$ molecules. This suggests a gradual substitution of $\rm H_2O$ molecules on the iron surface, leading to the formation of a stable layer capable of protecting the iron from aqueous corrosion.

It can also be noted that BI and NNBI exhibit high negative adsorption energy during the simulation process, which indicates a stable and stronger adsorption of these inhibitors on a steel surface.⁵⁸

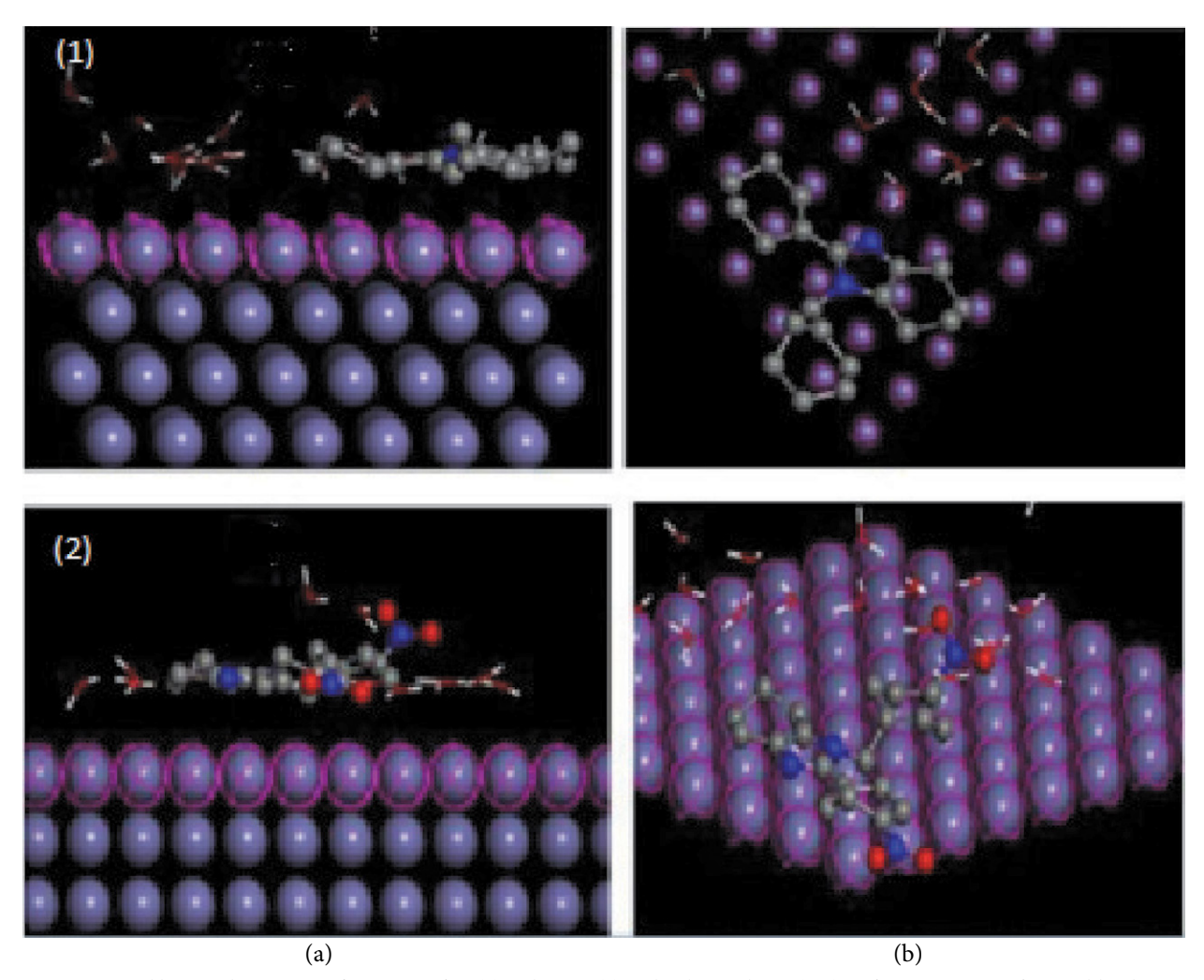


Figure 13. Equilibrium adsorption configurations of BI (1) and NNBI (2) molecules on the Fe (110) surface in presence of water, (a) side view (b) top view.

Table 9. Molecular dynamics simulation (MDS) results for the lowest adsorption configurations of BI and NNBI compounds on the Fe $(110)/50~H_2O$ interface.

Systems		BI/Fe (110)/H ₂ O	NNBI/Fe (110)/H ₂ O
Total energy (E_t)	(kJ/mol)	-845	-891
Adsorption energy (E_{ads})	(kJ/mol)	-1929	-2116
Rigid adsorption energy	(kJ/mol)	-899	-924
Deformation energy (D_E) (kJ/mol)	-1029	-1191
dE_{ads}/dN_i compounds	(kJ/mol)	218	409
dE_{ads}/dN_iH_2O	(kJ/mol)	-35	-33

4. Conclusion

Two new benzimidazole derivatives namely 1-Benzyl-2-phenyl 1H-benzimidazole (BI) and1-(4-Nitrobenzyl)-2-(4-nitrophenyl)-1H-benzimidazole (NNBI) were investigated as corrosion inhibitors for mild steel in 1 M HCl medium using a combined experimental and theoretical approaches.

The electrochemical analysis revealed that the inhibition efficiency of both inhibitors increases as their concentration increase according to the sequence BI > NNBI, the substitution with the nitro electron-withdrawing group (NO₂) reduces the protective power of NNBI. EIS plots indicated that the addition of inhibitors increases the charge-transfer resistance of the corrosion process, and hence the inhibition performance. The outcomes obtained from potentiodynamic polarization data indicate that the investigated compounds are mixed type inhibitors. The inhibitors adsorption on the metal surface follow the Langmuir isotherm model which is attributed to the monolaver formation of the inhibitors molecules on the steel surface. The obtained values of kinetic and thermodynamic parameters (E_a , ΔG_{ads}°) suggest that the adsorption process of BI and NNBI on mild steel surface in 1 M HCl occurred by physical and chemical ways.

The data achieved by electrochemical techniques corroborate. The inhibition rates determined are close and evolve in the same way. The inhibitory effectiveness of the two benzimidazole derivatives is confirmed even at high temperatures, indicating their strong thermostability.

Quantum chemical calculations extend the understanding of the experimental findings and show that heteroatoms and aromatic backbones play a crucial role in adsorption process thus a correlation between the inhibition efficiency and the molecular structure of the two inhibitors was established.

Molecular dynamics simulation (MDS) indicates that both investigated molecules adsorb in a parallel manner to the steel surface suggesting a better surface coverage of the metal and the high negative adsorption energies of BI and NNBI indicates their spontaneous and stronger adsorption on the steel surface. The computational studies confirmed experimental results.

This work provides a step forward the best understanding of the role of two benzimidazole derivatives as new efficient corrosion inhibitors for steel corrosion in 1 M HCl medium and their behavior could be assessed with similar compounds in order to step up the search for more efficient organic corrosion inhibitors.

Authors' contributions:

S. B. and L. T. conceived and designed the experiments; S. B. and L. T. performed the experiments and analyzed the data; S. B. and L. T. revised the paper.

CRediT authorship contribution statement:

This statement is to certify that all Authors of the article "Inhibition effect of benzimidazole derivatives on the corrosion of mild steel in acidic medium: Experimental and theoretical studies" have approved the manuscript being submitted. We warrant that the article is original and has not received prior publication and is not under consideration for publication elsewhere.

Declaration of Competing Interest

The authors declare no conflict of interest.

Data Availability: upon reasonable request by contacting the corresponding author(s).

Funding

This research received no external funding.

5. References

- M. Yadav, S. Kumar, T. Purkait, L. O. Olasunkanmi, I. Bahadur, E. E. Ebenso, *J. Mol. Liq.* 2016, 213, 122–138.
 DOI:10.1016/j.molliq.2015.11.018
- E. E. Ebenso, I. B. Obot, L. C. Murulana, Int. J. Electrochem. Sci.
 2010, 5, 1574–1586. DOI:10.1016/S1452-3981(23)15412-5
- 3. Y. Tang, F. Zhang, S. Hu, Z. Cao, Z. Wu, W. Jing, *Corros. Sci.* **2013**, *74*, 271–282. **DOI**:10.1016/j.corsci.2013.04.053
- L. Toukal, M. Foudia, D. Haffar, N. Aliouane, M. Al-Noaimi,
 Y. Bellal, H. Elmsellem, I. Abdel-Rahman, J. Indian Chem.
 Soc. 2022, 99, 100634. DOI:10.1016/j.jics.2022.100634
- C. Lee, W. Yang, R. G. Parr, *Phys. rev. B.* 1988, *37*, 785–789.
 DOI:10.1103/PhysRevB.37.785
- M. Frisch, G. Trucks, H. Schlegel, G. Scuseria, M. Robb, J. Cheeseman, G. Scalmani, V. Barone, B. Mennucci, G. Petersson, Gaussian 09, Revision A. 1, Gaussian Inc., Wallingford, CT., 2009.

- N. Metropolis, A. W. Rosenbluth, M. N. Rosenbluth, A. H. Teller, E. Teller, *J. Chem. Phys.* 1953, 21, 1087.
 DOI:10.1063/1.1699114
- 8. F. El Hajjaji, I. Merimi, M. Messali, R. J. Obaid, R. Salim, M. Taleb, B. Hammouti, *Mater. Today Proc.* **2019**, *13*, 822–831. **DOI**:10.1016/j.matpr.2019.04.045
- C. Boulechfar, H. Ferkous, S. Djellali, M. A. Amin, S. Boufas, A. Djedouani, A. Delimi, Y. Ben Amor, K. Kumar Yadav, B. H. Jeon, Y. Benguerba, *J. Mol. Liq.* 2021, 344, 117874.
 DOI:10.1016/j.molliq.2021.117874
- S. Prifiharni, G. Mashanafie, G. Priyotomo, A. Royani, A. Ridhova, B. Elya, J. W. Soedarsono, *J. Indian Chem. Soc.* **2022**, 99, 100520. **DOI**:10.1016/j.jics.2022.100520
- R. Khanna, V. Kalia, R. Kumar, R. kumar, P. Kumar, H. Dahiya, P. Pahuja, G. Jhaa, H. Kumar, J. Mol. Struct. 2024, 1297, 136845. DOI:10.1016/j.molstruc.2023.136845
- S. Abdoune, N. Aliouane, A. Hellal, M. Al-Noaimi, N. Sait, N. Chafai, L. Toukal, N. Ait Ahmed, *J. Mol. Struct.* 2024, 1295, 136673. DOI:10.1016/j.molstruc.2023.136673
- W. Ettahiri, M. Adardour, E. Ech-chihbi, M. Azam, R. Salim,
 S. Dalbouha, K. Min, Zakia Rais, A. Baouid, M. Taleb, *Colloids Surf. A Physicochem. Eng. Asp.* 2024, 681, 132727.
 DOI:10.1016/j.colsurfa.2023.132727
- T. Yan, S. Zhang, L. Feng, Y. Qiang, L. Lu, D. Fu, Y. Wen, J. Chen, W. Li, B. Tan, J. Taiwan Inst. Chem. Eng. 2020, 106, 118–129. DOI:10.1016/j.jtice.2019.10.014
- 15. D. Daoud, H. Hamani, T. Douadi, *J. Adhes. Sci. Technol.* **2021**, 35, 2319–2345. **DOI:**10.1080/01694243.2021.1885923
- Q. Wang, X. Wu, H. Zheng, X. Xiao, L. Liu, Q. Zhang, P. Gao,
 Z. Yan, Y. Sun, Z. Li, X. Li, Colloids Surf. A Physicochem. Eng.
 Asp. 2022, 640, 128458. DOI:10.1016/j.colsurfa.2022.128458
- 17. D. S. Zinad, M. Hanoon, R. D. Salim, S. I. Ibrahim, A. A. Al-Amiery, M. S. Takriff, A. A. H. Kadhum, *Int. J. Corros. Scale Inhib.* **2020**, *9*, 228–243.
 - **DOI:** 10.17675/2305-6894-2020-9-1- 14.
- A. Alamiery, L. M. Shaker, T. Allami, A. H. Kadhum, M. S. Takriff, *Mater. Today Proc.* 2021, 44, 2337–2341.
 DOI:10.1016/j.matpr.2020.12.431
- 19. M. Husaini, U. Bishir, I. M.Adamu, I. M. Bashir, *Res. J. Chem. Environ.* **2020**, *24*, 99–106.
- 20. M. Mahdavian, M. M. Attar, *PCCC*. **2015**, *8*, 177–196. **DOI**:10.1590/s1517-707620210002.1278
- A. Ziouani, S. Atia, H. Hamani, T. Douadi, M. Al-Noaimi, N. Gherraf, *J. Indian Chem. Soc.* 2023, 100, 100832.
 DOI:10.1016/j.jics.2022.100832
- 22. M. Oubaaqa, M. Ouakki, M. Rbaa, F. Benhiba, M. Galai, R. Idouhli, M. Maatallah, A. Jarid, I. Warad, B. Lakhrissi, A. Zarrouk, M. EbnTouhami, J. Phys. Chem. Solids 2022, 169, 110866. DOI:10.1016/j.jpcs.2022.110866
- N. Sait, N. Aliouane, N. Ait Ahmed, L. Toukal, M. Al-Noaimi, J. Adhes. Sci. Technol. 2022, 36, 109–133.
 DOI:10.1080/01694243.2021.1916250
- S. Boukazoula, D. Haffar, R. Bourzami, L. Toukal, V. Dorcet, *J. Mol. Struct.* 2022, *1261*, 132852.
 DOI:10.1016/j.molstruc.2022.132852
- 25. L. Raisemche, I. Kaabi, T. Douadi, M. Al-Noaimi, A. Alrashed,

- M. S. Mubarak, N. Elboughdiri, A. Zouaoui, Y. Benguerba, *J. Environ. Chem. Eng.* **2024**, *12*, 112354. **DOI:**10.1016/j.jece.2024.112354
- A. Boutouil, I. Elazhary, M. R. Laamari, H. Ben El Ayouchia,
 H. Anane, M. El Had- dad, S. E. Stiriba, *J. Adhes. Sci. Technol.* 2020, 34, 549–578. DOI:10.1080/01694243.2019.1681741
- R. Haldhar, D. Prasad, N. Mandal, F. Benhiba, I. Bahadur, O. Dagdag, Colloids Surf. A Physicochem. Eng. Asp. 2021, 614, 126211. DOI:10.1016/j.colsurfa.2021.126211
- 28. P. R. Ammal, A. R. Prasad, A. Joseph, Egypt. J. Pet. 2018, 27, 1067–1076. DOI:10.1016/j.ejpe.2018.03.006
- 29. N. Bounedjar, M. Fouad Ferhat, L. Toukal, R. Messai, *Mater. Chem. Phys.* **2024**, *311*, 128555.
 - DOI:10.1016/j.matchemphys.2023.128555 M. Alahiane, R. Oukhrib, Y. AitAlbrimi, H. Ab
- M. Alahiane, R. Oukhrib, Y. AitAlbrimi, H. AbouOualid, H. Bourzi, R. AitAkbour, A. Assabbane, A. Nahle, M. Hamdani, RSC Adv. 2020, 10, 41137–41153.
 DOI:10.1039/D0RA06742C
- M. Galai, M. Rbaa, M. Ouakki, K. Dahmani, S. Kaya, N. Arrousse, N. Dkhireche, S. Briche, B. Lakhrissi, M. EbnTouhami, *Chem. Phys. Lett.* 2021, 776, 138700.
 DOI:10.1016/j.cplett.2021.138700
- 32. N. B. Iroha, V. C. Anadebe, N. J. Maduelosi, L. A. Nnanna, L. C. Isaiah, O. Dagdag, A. Berisha, E. E. Ebenso, *Colloids Surf. A Physicochem. Eng. Asp.* 2023, 660, 130885.
 DOI:10.1016/j.colsurfa.2022.130885
- S. Benabid, T. Douadi, S. Issaadi, C. Penverne, S. Chafaa, *Measurement* 2017, 99, 53–63.
 DOI:10.1016/j.measurement.2016.12.022
- V. Shenoy K, P. P. Venugopal, P. D. ReenaKumari, D. Chakraborty, *Mater. Chem. Phys.* 2022, 281, 125855.
 DOI:10.1016/j.matchemphys.2022.125855
- 35. N. N. Hau, D. Q. Huong, *J. Mol. Struct.* **2023**, *1277*, 134884. **DOI:**10.1016/j.molstruc.2022.134884
- F. H. Zaidon, K. Kassim, H. M. Zaki, Z. Embong, N. Z. N. Hashim, *J. Mol. Liq.* 2021, 329, 115553.
 DOI:10.1016/j.molliq.2021.115553
- S. A. Al Kiey, A. A. El-Sayed, A. M. Khalil, *Colloids Surf. A Physicochem. Eng. Asp.* 2024, 683, 133089.
 DOI:10.1016/j.colsurfa.2023.133089
- E. Ech-chihbi, R. Salim, M. Ouakki, M. Koudad, L. Guo, M. Azam, N. Benchat, Z. Rais, M. Taleb, *Mater. Today Sustain*.
 2023, 24, 100524. DOI:10.1016/j.mtsust.2023.100524
- A. Saady, Z. Rais, F. Benhiba, R. Salim, K. Alaoui, N. Arrousse, F. Elhajjaji, M. Taleb, K. Jarmoni, Y. Rodi, I. Warad, A. Zarrouk, *Corros. Sci.* 2021, 189, 109621.
 DOI:10.1016/j.corsci.2021.109621
- M. Ouakki, M. Galai, Z. Benzekri, Z. Aribou, E. Ech-Chihbi, L. Guo, K. Dahmani, K. Nouneh, S. Briche, S. Boukhris, M. Cherkaoui, J. Mol. Liq. 2021, 344, 117777.
 DOI:10.1016/j.molliq.2021.117777
- O. Moumeni, M. Mehri, R. Kerkour, A. Boublia, F. Mihoub, K. Rebai, A. Ali Khan, A. Erto, A. S. Darwish, T. Lemaoui, N. Chafai, Y. Benguerba, J. Taiwan Inst. Chem. Eng. 2023, 147, 104918. DOI:10.1016/j.jtice.2023.104918
- 42. H. Hamani, D. Daoud, S. Benabid, T. Douadi, J. Indian Chem.

- Soc. 2022, 99, 100492. DOI:10.1016/j.jics.2022.100492
- 43. K. V. Shenoy, P. P. Venugopal, P. D. R. Kumari, D. Chakraborty, *Mater. Chem. Phys.* **2022**, *281*, 125855.
 - DOI:10.1016/j.matchemphys.2022.125855
- 44. L. Toukal, D. E. Belfennache, M. Foudia, R. Yekhlef, F. Benghanem, B. Hafez, H. Elmsellem, I. Abdel-Rahman, *Int. J. Corros. Scale Inhib.* **2022**, *11*, 438–464.
 - **DOI:**10.17675/2305-6894-2022-11-1-26
- P. P. Kumari, G. Anusha, J. N Cheerlin Mishma, R. K. Sinha,
 A. S. Suvarna, S. L. Gaonkar, *Heliyon* 2023, 9, e21014.
 DOI:10.1016/j.heliyon.2023.e21014
- M. Al-Noaimi, S. Benabid, H. Hamani, Q. F. A. Salman, M. Binsabt, F. F. Awwadi, K. Douadi, T. Douadi, *Chem. Data Collect.* 2022, 40, 100877. DOI:10.1016/j.cdc.2022.100877
- P. R. Ammal, M. Prajila, A. Joseph, J. Environ. Chem. Eng. 2018, 6, 1072–1085. DOI:10.1016/j.jece.2018.01.031
- 48. A. Dutta, S. Kr. Saha, U. Adhikari, P. Banerjee, D. Sukul, *Corros. Sci.* **2017**, *123*, 256–266.
 - **DOI:**10.1016/j.corsci.2017.04.017
- 49. W. M. I. W. M. Kamaruzzaman, M. S. Shaifudin, N. A. M. Nasir, M. A. Badruddin, N. Yusof, A. Adnan, N. Abdul Aziz, W. M. N. W. Nik, J. Haque, M. Murmu, P. Banerjee, M. S. M. Ghazali, *Mater. Chem. Phys.* 2024, 312, 128642.
 DOI:10.1016/j.matchemphys.2023.128642
- Ö. Uguz, M. Gümüs, Y. Sert, I. Koca, A. Koca, J. Mol. Struct.
 2022, 1262, 133025. DOI:10.1016/j.molstruc.2022.133025

- A. A. Abdulridha, M. A. A. H. Allah, S. Q. Makki, Y. Sert, H. Edan Salman, A. A. Balakit, *J. Mol. Liq.* 2020, *315*, 113690.
 DOI:10.1016/j.molliq.2020.113690
- M. A. Abbas, M. A. Bedair, O. E. El-Azabawy, E. S. Gad, ACS Omega 2021, 6, 15089–15102.
 DOI:10.1021/acsomega.1c01274
- 53. Y. El Aoufir, Y. El Bakri, H. Lgaz, A. Zarrouk, R. Salghi, I. Warad, Y. Ramli, A. Guenbour, E. M. Essassi, H. Oudda, J. Mater. Environ. Sci. 2017, 8, 3290–3302
- Z. Salarvand, M. Amirnasr, M. Talebian, K. Raeissi, S. Meghdadi, *Corros. Sci.* 2017, *114*, 133–145.
 DOI:10.1016/j.corsci.2016.11.002
- M. Yadav, D. Behera, S. Kumar, R. R. Sinha, *Ind. Eng. Chem. Res.* 2013, 52, 6318–6328. DOI:10.1021/ie400099q
- 56. Z. Rouifi, M. Rbaa, A. S. Abousalem, F. Benhiba, T. Laabaissi, H. Oudda, B. Lakhrissi, A. Guenbour, I. Warad, A. Zarrouk, Surf. Interfaces 2020, 18, 100442. DOI:10.1016/j.surfin.2020.100442
- H. EL Hassouni, A. Elyousfi, F. Benhiba, N. Setti, A. Romane,
 T. Benhadda, A. Zarrouk, A. Dafali, *Inorg. Chem. Commun.* 2022, 143, 109801. DOI:10.1016/j.inoche.2022.109801
- 58. E. H. Akroujai, S. Chetioui, N. Benzbiria, A. Barrahi, A. Chraka, A. Djedouani, S. Chtita, B. Dikici, I. Warad, A. Bellaouchou, M. Assouag, A. Zarrouk, *Int. J. Corros. Scale Inhib.* 2023, 12, 1441–1475.

DOI:10.17675/2305-6894-2023-12-4-5

Povzetek

Z uporabo elektrokemijske impedančne spektroskopije (EIS) in potenciodinamične polarizacije (PDP) smo ocenili učinek dveh heterocikličnih spojin, derivatov benzimedazola (BnZ), in sicer 1-benzil-2-fenil-1H-benzimedazola (BI) ter 1-(4-nitrobenzil)-2-(4-nitrofenil)-1H-benzimedazola (NNBI), na korozijo ogljikovega jekla v mediju 1M HCl. Proučevali smo vpliv koncentracije in temperature. Določeni elektrokemijski parametri so pokazali, da sta oba inhibitorja mešanega tipa. Inhibicijska učinkovitost NNBI je bila manjša od učinkovitosti BI. Najbolj elektronsko privlačna substituenta zagotavlja najnižjo učinkovitost. Mehanizem delovanja teh inhibitorjev smo ovrednotili s termodinamično študijo. Izračunane vrednosti , inso potrdile, da se BI in NNBI adsorbirata s kemijskim in fizikalnim procesom. Proces adsorpcije je spontan in sledi Langmuirovi adsorpcijski izotermi. Kvantno kemijski parametri, izračunani z uporabo teorije gostotnega funkcionala in simulacije molekularne dinamike, so potrdili tako eksperimentalne podatke kot tudi podatke iz literature.



Except when otherwise noted, articles in this journal are published under the terms and conditions of the Creative Commons Attribution 4.0 International License